ON THE COGGING TORQUE REDUCTION CAPABILITY OF FRACTIONAL-SLOT PM MACHINES

Ghada BEN HAMADOU **Ahmed MASMOUDI**
Research Unit on Renewable Energies and Electric Vehicles
University of Sfax, Sfax Engineering School, BP W, 3038 Sfax, Tunisia
E-mail: ghadabh@gmail.com, a.masmoudi@enis.rnu.tn

Mongi BEN HAMADOU
University of Sfax, Sfax Faculty of Sciences, BP W, 3038 Sfax, Tunisia
E-mail: mongi.benhamadou@fss.rnu.tn

Abstract: *The paper is devoted to an investigation of the cogging torque exhibited by two brushless surface mounted PM machines which share the same rotor topology and differ by the slot per pole and per phase: (i) a unity one and (ii) a fractional one equal to* $2/5$ *which has been found a viable candidate to achieve many interesting features especially a high torque production capability with a reduced cogging torque. In a first step, an analytical formulation of the cogging torque is derived, then applied to predict the cogging torques of both machines. It has been found that the machine with a fractional slot per pole and per phase produces a lower cogging torque. Finally, a 2D FEA validation of the analytical results is provided combined with the computation of the electromagnetic torques developed by both machines.*

Keywords: *Fractional-slot permanent magnet machines, cogging torque, analytical formulation, finite element analysis, comparison.*

1. Introduction

Most if not all topologies of permanent magnet machines suffer more or less from the torque oscillation due to the interaction between the PMs located in one side of the air gap and the magnetic circuit teeth located in the other side, yielding the so-called "cogging torque".
Many works have been reported in the literature regarding the assessment of cogging torque. Some authors proposed analytical models based on the virtual work method [1], [2], [3]. Others presented models based on the Maxwell stress method [4], [5]. The use of combined analytical-FEA methods have also been extensively treated [6], [7].
The established models are commonly developed for the sake of the cogging torque reduction. This latter represents a state of the art topic. The world-wide reported cogging torque reduction technique is the skewing, [4], [9], [8], [10], with a one-slot pitch of either the PMs or the teeth in the case of integer-slot PM machines.
Nevertheless, the skewing remains a penalty for the machine manufacturability. This drawback could be by-passed considering fractional-slot permanent magnet machines where the skewing turns to be useless if suitable slot/pole combinations are selected.
The growing interest in fractional-slot permanent magnet machines is also due to [15], [14], [13], [11], [12]:

- ◇ their short end-winding leading to reduced copper losses and improved compactness, especially when double-layer slots are considered,
- ◇ their high slot fill factor especially when coupled to segmented stator structures,
- ◇ their interesting fault-tolerance capabilities thanks to their low mutual inductances, especially when single-layer slots are considered.

Recently, *Zhu* et al. [16], proposed an analytical approach based on a subdomain model for the computation of the open-circuit magnetic field in surface-mounted permanent-magnet machines with any pole and slot combinations, including fractional slot machines.
The present work develops the *Zhu* approach to investigate the cogging torque exhibited by two brushless surface mounted PM machines which share the same rotor topology and differ by the slot per pole and per phase.

2. Cogging Torque Formulation

Let us apply the approach developed by *Zhu* et al. [16] to a 12 slots/10 poles surface mounted PM machine whose cross-section is illustrated in figure 1.

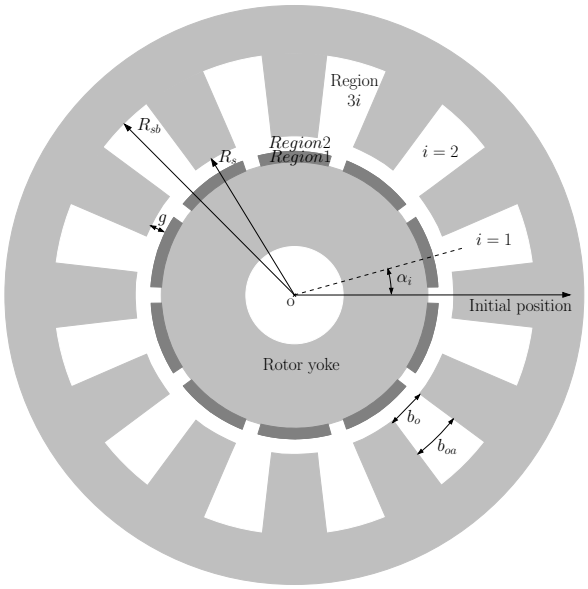

Fig. 1: Layout of a 12 slots/10 poles surface mounted PM machine highlighting three types of subdomains

The magnets are surface mounted and radially magnetized. Prior to deal with the analytical model, the following assumptions are accounted for in order to simplify the electromagnetic phenomena [16]:

- simplified stator slot shape,
- stator and rotor iron infinite permeability,
- neglected end effect,
- non conductive magnet material,
- magnet linear demagnetization.

The exact subdomain model consists in dividing the whole study domain of the field problem into three types of subdomains [16], such that: magnet (Region 1), air-gap (Region 2), and stator slots (Region 3) ($i = 1, 2, ...N_s$). Then, by applying the boundary conditions into the scalar potential distributions in polar coordinates for each sub-region, taking into consideration the influence of interaction between slot openings, one can obtain the air gap flux density expression.

Let's remind the general formulation of the scalar potential distributions expressed in terms of the polar coordinates (r, α), in the case of Region 1 and for multipolar machines [16]:

$$\phi_1(k \neq 1) = \sum_k \Gamma_1(k,r)\cos(k\alpha) + \Lambda_1(k,r)sin(k\alpha) \quad (1)$$

where:

$$\begin{cases} \Gamma_1(k,r) &= A_1(k)r^k + B_1(k)r^{-k} + \dfrac{M_{ck}r}{\mu_r(1-k^2)} \\ \Lambda_1(k,r) &= C_1(k)r^k + D_1(k)r^{-k} + \dfrac{M_{sk}r}{\mu_r(1-k^2)} \end{cases} \quad (2)$$

and in the case of Region 2 [16]:

$$\phi_2(k \neq 1) = \sum_k \Gamma_2(k,r)\cos(k\alpha) + \Lambda_2(k,r)sin(k\alpha) \quad (3)$$

where:

$$\begin{cases} \Gamma_2(k,r) &= A_2(k)r^k + B_2(k)r^{-k} \\ \Lambda_2(k,r) &= C_2(k)r^k + D_2(k)r^{-k} \end{cases} \quad (4)$$

and in the case of the i^{th} slot (Region $3i$) [16]:

$$\phi_{3i} = \sum_m C_{3i}(m)\left[\left(\frac{r}{R_{sb}}\right)^{F_m} - \left(\frac{r}{R_{sb}}\right)^{-F_m}\right] \times \sin\left[F_m\left(\alpha + \frac{b_{oa}}{2} - \alpha_i\right)\right] \quad (5)$$

where μ_r is the relative permeability of magnets, k and m are harmonic orders, R_{sb} is the radius of the slot bottom, $A_1(k)$ to $D_1(k)$, $A_2(k)$ to $D_2(k)$, and $C_{3i}(m)$ are coefficients to be determined by the boundary conditions, α_i is the position of the i^{th} slot, b_{oa} is the slot opening angle corresponding to the slot opening width b_o, and:

$$F_m = \frac{m\pi}{b_{oa}} \qquad \& \qquad b_{oa} = \frac{b_o}{R_s} \quad (6)$$

In what follows, let us focus on the rotor which is illustrated in figure 2

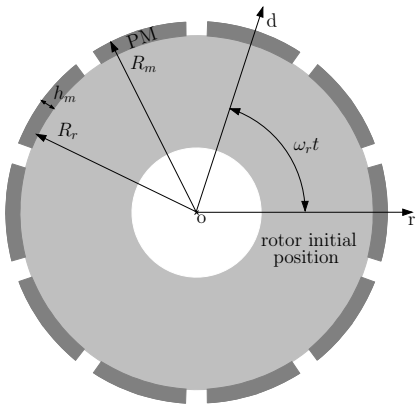

Fig. 2: Layout of the rotor of a 12 slots/10 poles surface mounted PM machine

The magnetization of magnets can be expressed as follows [16]:

$$\mathcal{M} \;=\; M_r\; r \;+\; M_\alpha\; \alpha \tag{7}$$

In the case of radial magnetization $M_\alpha = 0$, which yields:

$$M_r = \sum_{k=5,15,25,....} M_{rck}\cos(k\alpha) + M_{rsk}\sin(k\alpha) \tag{8}$$

where:

$$\begin{cases} M_{rck} &= M_{rk}\cos(k\omega_r t) \\ M_{rsk} &= M_{rk}\sin(k\omega_r t) \end{cases} \tag{9}$$

with:

$$M_{rk} = \frac{4p_r B_r}{k\pi\mu_0}\sin(\frac{k\pi\alpha_p}{2p_r}) \quad \frac{k}{p_r} = 1,3,5... \tag{10}$$

where μ_0 is the relative permeability of air, B_r is the magnet residual flux density and α_p is the pole arc to pole pitch ratio, ω_r is the rotor speed, and p_r is the rotor pole pair.
According to equation (3), the scalar potential on the surface of the stator bore ($r = R_s$) is:

$$\phi_2 = \sum_k \Gamma_2(k,R_s)\cos(k\alpha) + \Lambda_2(k,R_s)\sin(k\alpha) \tag{11}$$

Moreover, according to equation (5), the scalar potential on the surface of the stator bore can also be expressed as:

$$\phi_s = \begin{cases} \phi_{3i}(R_s) & \text{along the slot opening} \\ 0 & \text{otherwise} \end{cases} \tag{12}$$

where $\phi_{3i}(R_s)$ could be expressed as follows:

$$\phi_{3i}(R_s) = \sum_m C_{3i}(m)\chi_m \sin[F_m(\alpha + \frac{b_{oa}}{2} - \alpha_i)] \tag{13}$$

with:

$$\chi_m = (\frac{R_s}{R_{sb}})^{F_m} - (\frac{R_s}{R_{sb}})^{-F_m} \tag{14}$$

According to continuity condition, one can write:

$$\phi_2(R_s) = \phi_{3i}(R_s) \tag{15}$$

In order to solve equation (15), ϕ_{3i} can be expanded into *Fourier* series as:

$$\phi_s = \sum_k [A_s(k)\cos(k\alpha) + B_s(k)\sin(k\alpha)] \tag{16}$$

where:

$$\begin{cases} A_s(k) \;=\; \sum_i \sum_m C_{3i}(m)\chi_m \eta_{si}(m,k) \\ B_s(k) \;=\; \sum_i \sum_m C_{3i}(m)\chi_m \xi_{si}(m,k) \end{cases} \tag{17}$$

η_{si} and ξ_{si} are expressed as follows:

$$\begin{cases} \eta_{si} \;=\; \eta_s\cos(k\alpha_i) - \xi_s\sin(k\alpha_i) \\ \xi_{si} \;=\; \eta_s\sin(k\alpha_i) + \xi_s\cos(k\alpha_i) \end{cases} \tag{18}$$

where:

$$\eta_s = \begin{cases} \dfrac{2mb_{oa}\cos(kb_{oa}/2)\sin^2(m\pi/2)}{m^2\pi^2 - k^2 b_{oa}^2} & m\pi \neq kb_{oa} \\ \dfrac{b_{oa}}{2\pi}\sin(\dfrac{m\pi}{2}) & m\pi = kb_{oa} \end{cases} \tag{19}$$

and:

$$\xi_s = \begin{cases} -\dfrac{2mb_{oa}\sin(kb_{oa}/2)\cos^2(m\pi/2)}{m^2\pi^2 - k^2 b_{oa}^2} & m\pi \neq kb_{oa} \\ \dfrac{b_{oa}}{2\pi}\cos(\dfrac{m\pi}{2}) & m\pi = kb_{oa} \end{cases} \tag{20}$$

Accounting for the equation set (11)-(17), one can establish the following:

$$\begin{cases} A_s = A_2 R_s^k + B_2 R_s^{-k} = \sum_i \sum_m C_{3i}(m)\chi_m \eta_{si}(m,k) \\ B_s = C_2 R_s^k + D_2 R_s^{-k} = \sum_i \sum_m C_{3i}(m)\chi_m \xi_{si}(m,k) \end{cases} \tag{21}$$

Employing the boundary conditions considering an infinite permeability of the rotor yoke, continuous scalar potential, and radial flux density at ($r = R_m$) leads to the following harmonic coefficients of ϕ_2:

$$\begin{cases} A_2 = \dfrac{K_{Brc}}{-\mu_0 k}\dfrac{R_m^{k+1}}{R_s^{2k}} + B_{5k}A_{5k}A_s(k) \\ B_2 = \dfrac{K_{Brc}}{\mu_0 k}R_m^{k+1} - B_{6k}A_{6k}A_s(k) \\ C_2 = \dfrac{K_{Brs}}{-\mu_0 k}\dfrac{R_m^{k+1}}{R_s^{2k}} + B_{5k}A_{5k}B_s(k) \\ D_2 = \dfrac{K_{Brs}}{\mu_0 k}R_m^{k+1} + B_{6k}A_{6k}B_s(k) \end{cases} \tag{22}$$

where:

$$\begin{cases} K_{Brc} &= A_{4k}\gamma(k)M_{rck} \\ K_{Brs} &= A_{4k}\gamma(k)M_{rsk} \end{cases} \tag{23}$$

with in the case of an internal rotor machine:

$$\begin{cases} A_{4k} = -\dfrac{1}{2}\mu_0 k \\ \gamma \;\; = \dfrac{2}{k^2-1}\dfrac{1}{\rho}\left[(1-k) - 2\Big(\dfrac{R_r}{R_m}\Big)^{k+1} + (k+1)\Big(\dfrac{R_r}{R_m}\Big)^{2k}\right] \\ \rho \;\; = (\mu_r+1)\left[1-\Big(\dfrac{R_r}{R_s}\Big)^{2k}\right] - (\mu_r-1)\left[\Big(\dfrac{R_m}{R_s}\Big)^{2k} - \Big(\dfrac{R_r}{R_m}\Big)^{2k}\right] \\ B_{5k} = R_s^{-k} \\ B_{6k} = R_s^{-k}R_m^{2k} \\ A_{5k} = \dfrac{1}{\rho}\left[(\mu_r+1) + (\mu_r-1)\Big(\dfrac{R_r}{R_m}\Big)^{2k}\right] \\ A_{6k} = \dfrac{1}{\rho}\left[(\mu_r-1) + (\mu_r+1)\Big(\dfrac{R_r}{R_m}\Big)^{2k}\right] \end{cases}$$

The remaining harmonic coefficient $C_{3i}(m)$ of ϕ_{3i} could be calculated using the last boundary condition which considers a continuous radial component flux density at stator slot opening [16]. According to (22), the following equation set can be derived:

$$\begin{cases} A_2 R_s^{k-1} - B_2 R_s^{-k-1} &= G_1 - \lambda A_s(k) \\ C_2 R_s^{k-1} - D_2 R_s^{-k-1} &= G_2 - \lambda B_s(k) \end{cases} \quad (24)$$

with in the case of an internal rotor machine:

$$\begin{cases} G_1 &= (\frac{R_m}{R_s})^{k+1} \quad \gamma(k) M_{rck} \\ G_2 &= (\frac{R_m}{R_s})^{k+1} \quad \gamma(k) M_{rsk} \\ \lambda &= -\frac{1}{R_s} \quad [A_{5k} + (\frac{R_s}{R_m})^{2k} A_{6k}] \end{cases} \quad (25)$$

The harmonic coefficient $C_{3i}(m)$ can be obtained by solving [16]:

$$\begin{aligned} \delta_m C_{3i}(m) = & \sum_k k[G_1(k)\sigma_{si}(m,k) + G_2(k)\tau_{si}(m,k)] \\ & - \sum_k k\lambda(k)\sigma_{si}(m,k) \sum_l \sum_j C_{3l}(m)\chi_j \eta_{sl}(j,k) \\ & - \sum_k k\lambda(k)\tau_{si}(m,k) \sum_l \sum_j C_{3l}(m)\chi_j \xi_{sl}(j,k) \end{aligned} \quad (26)$$

where $j = 1, 2, 3..., M$, $l = 1, 2, 3..., N_s$, M is the highest harmonic order of the scalar potential distribution along the slot openings, and

$$\delta_m = \frac{F_m}{R_{sb}} \left[\left(\frac{R_s}{R_{sb}} \right)^{F_m - 1} + \left(\frac{R_s}{R_{sb}} \right)^{-F_m - 1} \right] \quad (27)$$

Equation (26) can be rewritten as follows:

$$\delta C_{3i} = Y_{si} - P_{si} \sum_{l=1}^{N_s} \eta_{sl}^T \chi C_{3l} - Q_{si} \sum_{l=1}^{N_s} \xi_{sl}^T \chi C_{3l} \quad (28)$$

where:

$$\begin{cases} \delta &= diag(\delta_1, \delta_2, ..., \delta_M) \\ C_{3i} &= [C_{3i}(1) \;\; C_{3i}(2) \;\; ... \;\; C_{3i}(M)]^T \\ \eta_{si} &= (\eta_{si}(m,n))_{M \times N} \\ \xi_{si} &= (\xi_{si}(m,n))_{M \times N} \\ Y_{si} &= \sigma_{si} K G_1 + \tau_{si} K G_2 \\ \sigma_{si} &= \frac{2\pi}{b_{oa}} \eta_{si} \\ \tau_{si} &= \frac{2\pi}{b_{oa}} \tau_{si} \\ K &= diag(5, 15, ..., K) \\ G_1 &= [G_1(1), G_1(2), ..., G_1(N)]^T \\ G_2 &= [G_2(1), G_2(2), ..., G_2(N)]^T \\ P_{si} &= \sigma_{si} K \lambda \\ Q_{si} &= \tau_{si} K \lambda \\ \lambda &= diag(\lambda(1), \lambda(2), ..., \lambda(N)) \\ \chi &= diag(\chi(1), \chi(2), ..., \chi(M)) \end{cases} \quad (29)$$

Equation (28) shows that the scalar potential distributions of all slots are coupled together. These have to be solved simultaneously to completely account for such a slot coupling. To do so, equation (28) is rewritten as:

$$\delta_t C_{3t} = Y_{st} - P_{st} \eta_{st}^T \chi_t C_{3t} - Q_{st} \xi_{st}^T \chi_t C_{3t} \quad (30)$$

where:

$$\begin{cases} \delta_t &= diag(\delta, \delta, ..., \delta)_{N_s \times N_s} \\ C_{3t} &= [C_{31}^T \;\; C_{32}^T \;\; ... \;\; C_{3N_s}^T]^T \\ Y_{st} &= [Y_{s1}^T \;\; Y_{s2}^T \;\; ... \;\; Y_{sN_s}^T]^T \\ \sigma_{st} &= [\sigma_{s1}^T \;\; \sigma_{s2}^T \;\; ... \;\; \sigma_{sN_s}^T]^T \\ \tau_{si} &= [\tau_{s1}^T \;\; \tau_{s2}^T \;\; ... \;\; \tau_{sN_s}^T]^T \\ \eta_{st} &= \frac{b_{oa}}{2\pi} \sigma_{st} \\ \xi_{st} &= \frac{b_{oa}}{2\pi} \tau_{st} \\ P_{st} &= \sigma_{st} K \lambda = [P_{s1}^T \;\; P_{s2}^T \;\; ... \;\; P_{sN_s}^T]^T \\ Q_{st} &= \tau_{st} K \lambda = [Q_{s1}^T \;\; Q_{s2}^T \;\; ... \;\; Q_{sN_s}^T]^T \\ \chi_t &= diag(\chi, \chi, ..., \chi)_{N_s \times N_s} \end{cases} \quad (31)$$

The coefficient $C_{3t}(m)$ can be obtained considering a variable change as:

$$C_{et} = \chi_t C_{3t} \quad (32)$$

Applying the above variable change to equation (30) yields:

$$C_{et} = (W_{et} - P_{st} \eta_{st}^T - Q_{st} \xi_{st}^T)^{-1} Y_{st} \quad (33)$$

where:

$$\begin{cases} C_{et} &= [C_{e1}^T \;\; C_{e2}^T \;\; ... \;\; C_{eN_s}^T]^T \\ W_{et} &= \delta_t \chi_t^{-1} \end{cases} \quad (34)$$

The harmonic of scalar potential distribution along the slot openings 17 can be rewritten as:

$$\begin{cases} A_s(k) &= \sum_i \sum_m C_{ei}(m) \eta_{si}(m,k) \\ B_s(k) &= \sum_i \sum_m C_{ei}(m) \xi_{si}(m,k) \end{cases} \quad (35)$$

The air-gap flux density can be expressed by [16]:

$$\begin{cases} B_{rg} = \sum_k B_{rck} \cos(k\alpha) + \sum_k B_{rsk} \sin(k\alpha) \\ B_{\alpha g} = \sum_k B_{\alpha ck} \cos(k\alpha) + \sum_k B_{\alpha sk} \sin(k\alpha) \end{cases} \quad (36)$$

where:

$$\begin{cases} B_{rck} &= K_{Brc} \, f_{Br} \;\; - \;\; g_{Br} \, A_s \\ B_{rsk} &= K_{Brs} \, f_{Br} \;\; - \;\; g_{Br} \, B_s \\ B_{\alpha ck} &= -K_{Brs} \, f_{B\alpha} \;\; - \;\; g_{B\alpha} \, B_s \\ B_{\alpha sk} &= K_{Brc} \, f_{B\alpha} \;\; + \;\; g_{B\alpha} \, A_s \end{cases} \quad (37)$$

with in the case of an internal rotor machine:

$$\begin{cases} f_{Br} = \left(\frac{r}{R_s}\right)^{k-1}\left(\frac{R_m}{R_s}\right)^{k+1}+\left(\frac{R_m}{r}\right)^{k+1} \\ f_{B\alpha} = -\left(\frac{r}{R_s}\right)^{k-1}\left(\frac{R_m}{R_s}\right)^{k+1}+\left(\frac{R_m}{r}\right)^{k+1} \end{cases} \quad (38)$$

and:

$$\begin{cases} g_{Br} = \Delta\left[\left(\frac{r}{R_s}\right)^{k-1}+\left(\frac{R_r}{R_s}\right)^{k-1}\left(\frac{R_r}{r}\right)^{k+1}\right] \\ g_{B\alpha} = \Delta\left[\left(\frac{r}{R_s}\right)^{k-1}-\left(\frac{R_r}{R_s}\right)^{k-1}\left(\frac{R_r}{r}\right)^{k+1}\right] \end{cases} \quad (39)$$

with $\Delta = \frac{2\mu_0\mu_r k}{R_s\rho}$.

Following the determination of the scalar potential distribution harmonics along the stator bore, the air-gap flux density distribution can be predicted using equations (36)−(37. Then, the cogging torque can be computed applying the *Maxwell* stress tensor, such that:

$$T_{cog} = \frac{\pi l_a r^2}{\mu_0}\sum_k (B_{rck}B_{\alpha ck} + B_{rsk}B_{\alpha sk}) \quad (40)$$

3. Case Study

This paragraph deals with the comparison of the cogging torques exhibited by two brushless surface mounted PM machines which share the same rotor topology and differ by the slot per pole and per phase: (i) a unity one, and (ii) a fractional one equal to 2/5. The selection of the slot/pole combination characterized by an $Spp = 2/5$ is related to several reasons including, particularly:

- a high winding factor of (0.966),
- a low magnetic force,
- a low cogging torque due to its high $LCM(N_s, 2p_r)$. It should be noted that the number of cogging torque periods per revolution is equal to the $LCM(N_s, 2p_r)$. The higher is the cogging torque frequency the lower is its amplitude.

The cross-sections of the studied machines are shown in figures 3 and 4, respectively. Table 1 gives the geometrical parameters shared by both machines. It is worth noting that these parameters are not selected by any sizing approach especially regarding cogging torque reduction.

Table 1: Geometrical SMPMM parameters

R_{exts}	117 mm	e_c	22 mm
R_{ints}	70.5 mm	δ	0.5 mm
R_{extr}	66 mm	h_{pm}	4 mm
R_{intr}	40 mm	β_{pm}	0.75
l_a	70 mm	β	0.5

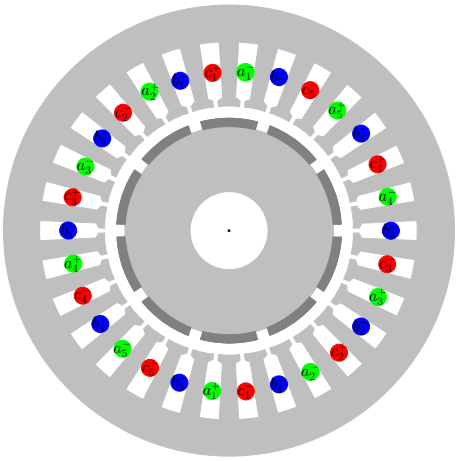

Fig. 3: 2D view of the unity S_{pp} surface mounted PM machine with $p_r = 5$ and $N_s = 30$

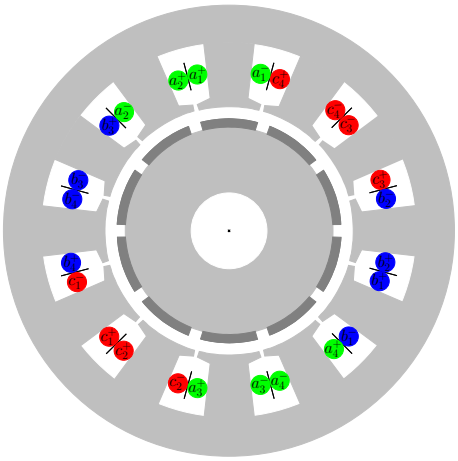

Fig. 4: 2D view of the fractional slot double-layer surface mounted PM machine with $p_r = 5$, $N_s = 12$, leading to $Spp = 2/5$

3.1 Analytical Model Based Assessment of the Cogging Torque

Figure 5 shows the analytically-predicted cogging torques exhibited by both machines under study, with the continuous line and the mark-line illustrate T_{cog} of the unity S_{pp} machine, and the fractional S_{pp} one, respectively.

One can notice that the peak-to-peak cogging torque is higher in the case of the integer-slot PM machine. It represents about the triple of the one of the fractional-slot PM machine. This could be explained by the fact that the frequency of the cogging torque of the integer-slot PM machine is lower and hence has higher magnitude. In other words, this is directly linked to the value of the $LCM(30, 10) = 30$, which is lower, compared to the one of the fractional-slot machine $LCM(12, 10) = 60$.

The results shown in figure 5 highlight the advantage of using fractional-slot concentrated windings in so far that they exhibit intrinsically low cogging torque.

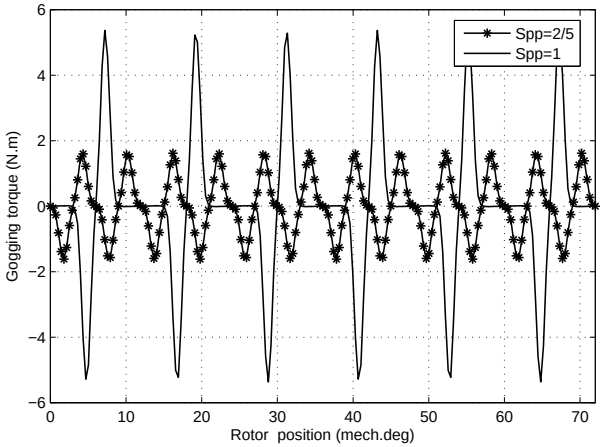

Fig. 5: Analytical cogging torque computed for both configurations: integer-slot distribution in continuous line and the fractional-slot distribution with mark-line distribution

3.2 Finite Element Analysis Based Assessment of the Cogging Torque

A. Case of Integer-Slot Machine

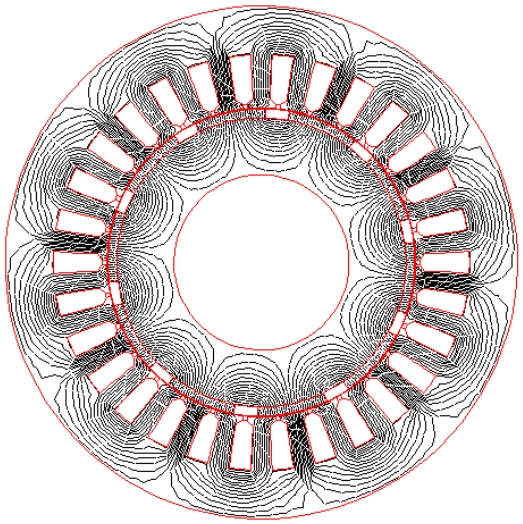

Fig. 6: No-load flux lines in a cross section of the magnetic circuit of the 30 slot/10 pole machine

Figure 6 shows the no-load flux lines in a cross section of the magnetic circuit of the 30 slot/10 pole machine.

Figure 7 illustrates the no-load flux density distribution in a cross section of the magnetic circuit of the 30 slot/10 pole machine.

Figure 8 shows, in continuous line, five periods of the cogging torque waveform computed by FEA. For the sake of comparison, the cogging torque waveform analytically-predicted, as shown in figure 5, is recalled in mark-line. Comparing both cogging torque waveforms reveals a good agreement, which confirms the effectiveness of the accuracy of the analytical model applied for the cogging torque prediction.

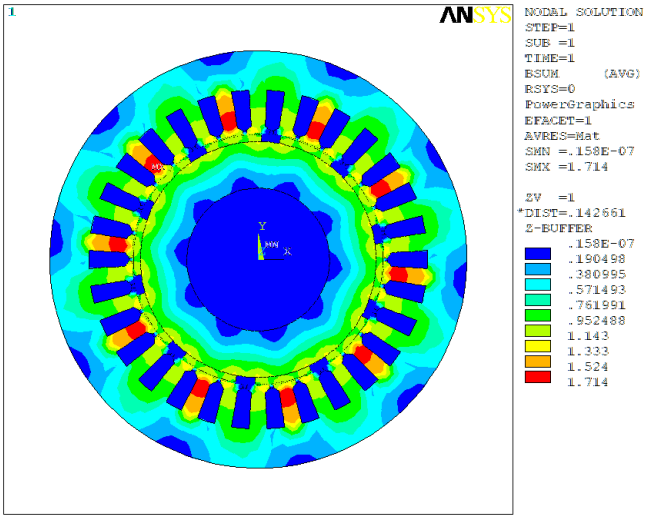

Fig. 7: No-load flux density distribution through a cross section of the magnetic circuit of the 30 slot/10 pole machine ($S_{pp} = 1$)

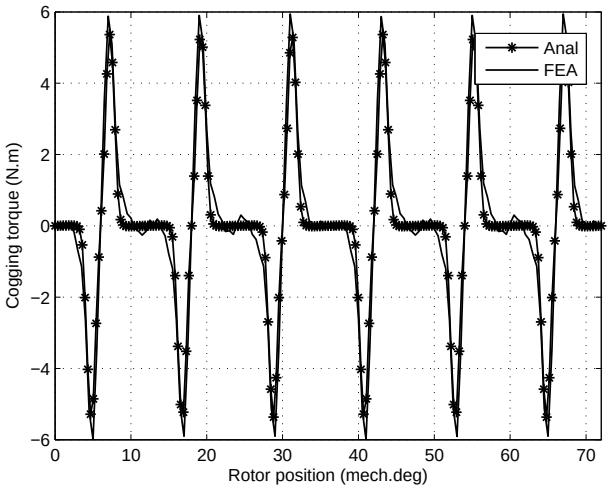

Fig. 8: Cogging torque waveform of the 30 slot/10 pole machine. Legend: (continuous line) FEA results, (mark-line) analytical results.

B. Case of fractional-Slot Machine

Figures 9 and 10 show the no-load flux lines and flux density map, respectively, in a cross section of the magnetic circuit of the 12 slot/10 pole machine.

Figure 11 illustrates, in continuous line, the cogging torque waveform computed by FEA, of the 12 slot/10 pole surface mounted PM machine and, in dashed-line, the one predicted by the analytical model.

One can notice that the cogging torques wiveforms computed by FEA and predicted by the analytical model are in good agreement. The peak-to-peak amplitude is almost equal to 3Nm while it is approximately equal to 12Nm in the case of 30 slot/10 pole machine.

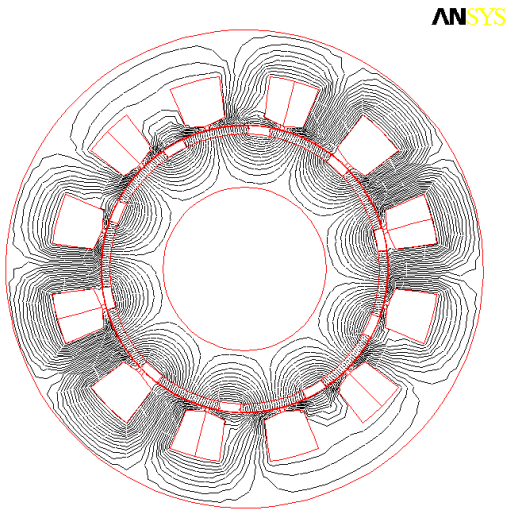

Fig. 9: No-load flux lines through a cross section of the magnetic circuit

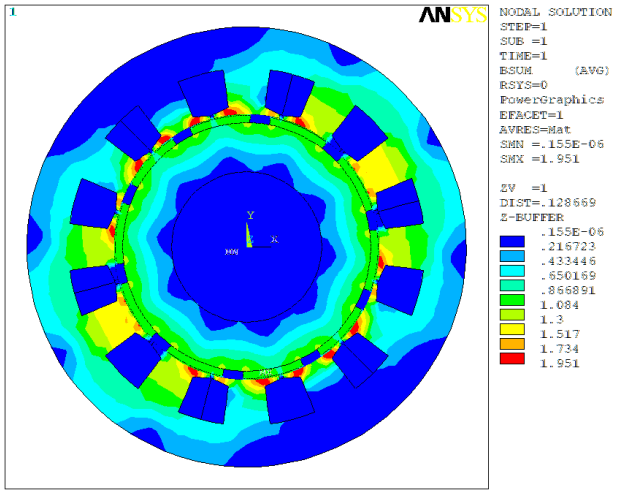

Fig. 10: No-load flux density map through a cross section of the magnetic circuit

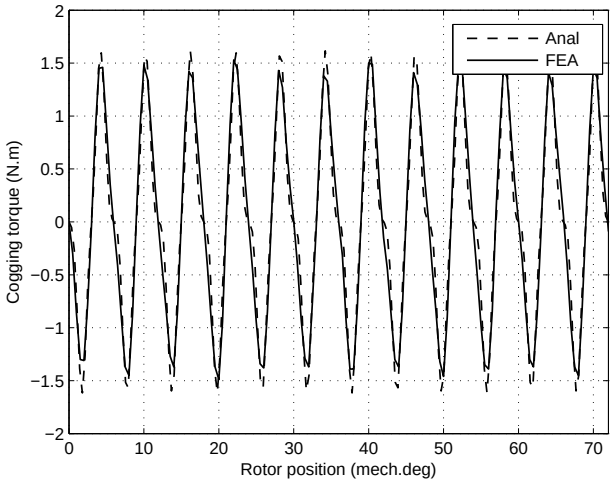

Fig. 11: Cogging torque of the 12 slot/10 pole machine. Legend: (continuous line) FEA results, (dashed-line) analytical results.

C. Extension of the Comparison to the Torque Production Capability

It has been clearly shown that the cogging torque amplitude exhibited by the fraction-slot machine is almost equal to the quarter of the integer-slot machine one. In order to extend the comparison to the torque production capability of both machines, the torque-angle characteristics have been computed by FEA and are illustrated in figure 12. One can notice that the fractional slot machine offers higher mean torque with lower ripple.

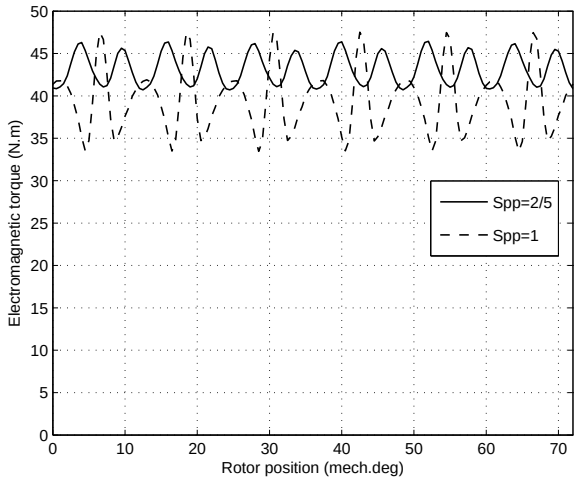

Fig. 12: Electromagnetic torque versus the mechanical angle considering a sinusoidal current supply with a current density of $6A/mm^2$, for both integer- and fractional-slot machines

4. Conclusion

The paper was devoted to an investigation of the cogging torques exhibited by two brushless surface mounted PM machines which share the same rotor topology and differ by their slot per pole and per phase, such that: (i) a unity one and (ii) a fractional one equal to 2/5.

An analytical model aimed at the prediction of the cogging torque was firstly developed. Then, it was applied to both machines. It has been found that the cogging torque amplitude exhibited by the fraction-slot machine is almost equal to the quarter of the integer-slot machine one.

Finally, a 2D FEA validation of the analytical results was provided combined with the electromagnetic torque computation. This has revealed that the fractional-slot machine has a better torque production capability.

References

[1] Y. Yang, X. Wang, R. Zhang, T. Ding, and R. Tang, "The optimization of pole arc coefficient to reduce cogging torque in surface-mounted permanent magnet motors," *IEEE Transactions on Magnetics*, vol. 42, no. 4, pp. 1135-1138, 2006.

[2] J. F. Gieras and M. E. Marler, "Analytical prediction of torque ripple in permanent magnet brushless motors," in Proc. *International Conference on Electric Machines* (ICEM02), Brugge, Belgium, pp. 33-34, 2002.

[3] J. de La Ree and N. Boules, "Torque production in permanent magnet synchronous motors," *IEEE Transactions on Industry Applications*, Vol. 25, no. 1, pp. 107-112, 1989.

[4] N. Bianchi and S. Bolognani, "Design techniques for reducing the cogging torque in surface-mounted PM motors," *IEEE Transactions on Industry Applications*, vol. 38, no. 5, pp. 1259-1265, 2002.

[5] D. Zarko, D. Ban, and T.A. Lipo, "Analytical solution of cogging torque in surface permanent-magnet motors using conformal mapping," *IEEE Transactions on Magnetics*, vol. 44, no. 1, pp. 52-65, 2008.

[6] C. Schlensok, M. Herranz Gracia, and K. Hameyer, "Combined numerical and analytical method for geometry optimization of a PM motor," *IEEE Transactions on Magnetics*, vol. 42, no. 4, pp. 1211-1214, 2006.

[7] J. Xintong, X. Jingwei, L. Yong, and L.Yongping, "Theoretical and simulation analysis of influences of stator toothWidth on cogging torque of BLDC motors," *IEEE Transactions on Magnetics*, vol. 45, no. 10, pp. 4601-4604, 2009.

[8] S. M. Hwang, J. B. Eom, Y. H. Jung, D. W. Lee, and B. S. Kang, "Various design techniques to reduce cogging torque by controlling energy variation in permanent magnet motors," *IEEE Transactions on Magnetics*, vol. 37, no. 4, pp. 2806-2809, Jul. 2001.

[9] T. M. Jahns and W. L. Soong, "Pulsating torque minimization techniques for permanent magnet ac motor drive-a review," *IEEE Transactions on Industry Electronics*, vol. 43, no. 2, pp. 321-330, 1996.

[10] M. Lukaniszyn, M. Jagiela, and R. Wrobel, "Optimization of permanent magnet shape for minimum cogging torque using a genetic algorithm," *IEEE Transactions on Magnetics*, vol. 40, no. 2, pp. 12281231, Mar. 2004.

[11] N. Bianchi, M. Dai Pre, L. Alberti and E. Fornasiero, "Theory and design of fractional-slot PM machines," Tutorial course notes, Industry Applications Society Annual Meeting, New Orleans, USA, September 2007.

[12] J. Cros and P. Viarouge, "Synthesis of high performance PM motors with concentrated windings," *IEEE Transaction on Energy Conversion*, vol. 17, pp. 248-253, 2002.

[13] Z.Q. Zhu, D. Ishak, D. Howe and J. Chen, "Unbalanced magnetic forces in permanent magnet brushless machines with diametrically asymmetric phase windings," *IEEE Transaction on Industry Applications*, vol. 43, no. 6, pp. 1544-1553, 2007.

[14] J. B. Wang, K. Atallah, Z. Q. Zhu, and D. Howe, "Modular 3-phase permanent magnet brushless machines for inwheel applications," *IEEE Trans. on Vehicular Technology*, vol.57, no. 5, pp. 2714-2720, 2008.

[15] G. Ben Hamadou, A. Masmoudi, I. Abdennadher and A. Masmoudi, "On the design of a single stator dual rotor permanent magnet machine," *IEEE Transaction on Magnetics*, Vol. 45, No. 1, pp. 127-132, 2009.

[16] Z.Q. Zhu, L.J. Wu,and Z.P. Xia , "An accurate subdomain model for magnetic field computation in slotted surface-mounted permanent-magnet machines," *IEEE Transactions on Magnetics*, vol. 46, no. 4, pp. 1100-1115, 2010.